

## Gain-Free Parity-Time Symmetry for Evanescent Fields

Huanan Li<sup>1</sup>, Ahmed Mekawy<sup>1,2</sup>, and Andrea Alù<sup>1,2,3,\*</sup><sup>1</sup>Photonics Initiative, Advanced Science Research Center, City University of New York, New York, New York 10031, USA<sup>2</sup>Department of Electrical Engineering, City College of The City University of New York, New York, New York 10031, USA<sup>3</sup>Physics Program, Graduate Center, City University of New York, New York, New York 10016, USA (Received 20 December 2020; accepted 4 June 2021; published 1 July 2021)

Parity-time (PT) symmetry, satisfied when a system commutes under combined parity and time-reversal operations, enables extreme optical responses in non-Hermitian systems with balanced distributions of gain and loss. In this Letter, we propose a different path for PT symmetry utilizing the evanescent field excitation of anti-PT-symmetric structures, which anticommute with the PT operator and do not necessarily require gain. Beyond offering a robust platform to explore PT symmetry, our study showcases an important link between non-Hermitian physics and near-field interactions, with implications in nanophotonics, plasmonics, and acoustics for nanoimaging, sensing, and communications.

DOI: [10.1103/PhysRevLett.127.014301](https://doi.org/10.1103/PhysRevLett.127.014301)

Under the general framework of non-Hermitian physics, parity-time (PT) symmetry has opened powerful opportunities [1] for intriguing wave manipulations not available in Hermitian setups. Such examples include robust wireless power transfer [2], anisotropic transmission resonances (ATR) and unidirectional invisibility [3–5], laser-absorber pairs [6–7], among several others. These features have been showcased in a wide range of classical settings, from photonics [8] and plasmonics [9–10] to metamaterials [11–13], as reviewed in [14]. As a different but related phenomenon, anti-PT symmetry has also been drawing increased attention in recent years. While PT-symmetric Hamiltonians commute with the joint parity-time operator, anti-PT-symmetric ones anticommute with it. In contrast with PT-symmetric systems, whose implementation requires a precise balance between loss and gain distributions [14], systems respecting anti-PT symmetry do not necessarily need gain [15–17], and support other interesting features, e.g., constant refraction [18], energy-difference conserving dynamics [19], and asymmetric mode switching for symmetry-broken modes [20]. Given their easier implementation, various experimental platforms realizing anti-PT symmetry have emerged in rapid succession in the past years, ranging from atomic vapors [21], electrical circuits [19], and diffusive systems [22], to coupled optical waveguides [20], microcavities [23], and optical fibers [24], offering different approaches to enable the required coupling mechanism for effective anti-PT-symmetric Hamiltonians. The lack of gain, however, prevents some of the most exciting features of PT-symmetric structures, as they are bounded by energy conservation and passivity constraints. These challenges are shared with recent proposals to observe phenomena reminiscent of PT symmetry in passive systems, by either modulating loss distributions in space [25,26] or by invoking slowly decaying modes [27].

Along a different research line, near-field wave physics has been extensively explored in the last decades [28], in connection with advances in near-field microscopy and nanofabrication techniques. Here, evanescent fields play a critical role, offering the possibility to go beyond the diffraction limit in imaging systems [29] and to surpass the blackbody limit in radiative heat transfer [30–37], with promising applications in thermophotovoltaics [38–41] and thermal management [42–44]. Also in acoustics, near-field physics has been offering interesting opportunities to engage the transverse spin of evanescent waves for near-field directional coupling [45–50], important for acoustic communications and sensing.

In this Letter, we explore the opportunities enabled by near-field physics and evanescent field excitations in anti-PT-symmetric systems. We find that effective steady-state PT-symmetric phenomena are enabled in these structures when excited by evanescent fields, overcoming the need for balanced loss and gain or for controlled release of stored energy [51–52], and overcoming the limitations of pseudo-PT-symmetric phenomena in passive systems [25–27]. Our study not only enriches near-field physics and provides new strategies for near-field manipulation based on PT symmetry in simple photonic setups, but it also opens a pathway to shed light into non-Hermitian phenomena using near-field technology.

*Scattering in anti-PT-symmetric coupled resonators systems.*—We start by considering a pair of coupled resonator optical waveguides (CROWs) [53–54] connected through two different coupled resonators, as sketched in Fig. 1(a). For convenience of notation, we set the zero frequency to the resonator frequency in the CROWs. The resulting dispersion relation is  $\omega = -2 \cos k$  with angular frequency  $\omega$  and wave number  $k$  in units of the interresonator coupling coefficient and the inverse of the CROW

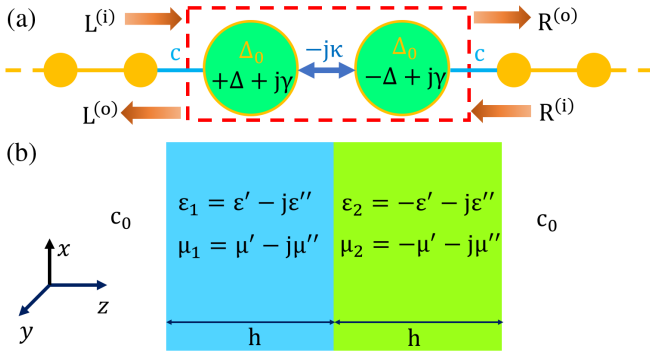


FIG. 1. Schematics of anti-PT-symmetric (a) coupled resonators and (b) photonic heterostructures.

period, respectively. In addition, the scattering problem at the two ports is described by the effective Hamiltonian  $H_{\text{eff}} = \Delta_0 I_2 + H^{(\text{APT})}$ , where  $\Delta_0$  is the common offset of the scatterer,  $I_2$  is a  $2 \times 2$  identity matrix, and  $H^{(\text{APT})} = \begin{pmatrix} \Delta + j\gamma & -jk \\ -jk & -\Delta + j\gamma \end{pmatrix}$ . The coefficient  $\gamma > 0$  is the damping frequency, identical in the two resonators, while the resonance frequencies are detuned from each other as  $\Delta_0 \pm \Delta$ . We assume an imaginary coupling  $-jk$  with  $\kappa > 0$  implemented, e.g., through resistive coupling [19,55], or generally through an auxiliary non-Hermitian cluster [59]. The scatterer obeys anti-PT symmetry, since  $H^{(\text{APT})}$  satisfies the anticommutation relation  $\{H^{(\text{APT})}, PT\} = 0$  with the parity operator  $P \equiv \begin{pmatrix} 0 & 1 \\ 1 & 0 \end{pmatrix}$  and the time-reversal operator  $T$  performing complex conjugation. The coupling strength between the scatterer and the left and right CROW ports is equal to  $c$ .

The *generalized* scattering matrix  $S$  [60] relates the signal amplitudes traveling toward and away from the scatterer from the left and right CROW ports, i.e.,  $\begin{pmatrix} L^{(o)} \\ R^{(o)} \end{pmatrix} = S \begin{pmatrix} L^{(i)} \\ R^{(i)} \end{pmatrix} \equiv \begin{pmatrix} r_L & t_{LR} \\ t_{RL} & r_R \end{pmatrix} \begin{pmatrix} L^{(i)} \\ R^{(i)} \end{pmatrix}$ . Using the method introduced in [61], we can obtain the explicit form of the  $S$  matrix for  $e^{i\omega t}$  time dependence as [62]

$$S = -I_2 - 2jc^2 \sin k \left[ \omega \left( 1 - \frac{1}{2}c^2 \right) I_2 - H_{\text{eff}} - jc^2 \sin k I_2 \right]^{-1}, \quad (1)$$

where  $\sin k = \sqrt{4 - \omega^2}/2$  for propagating waves when  $\omega \in (-2, 2)$  and  $\sin k = \mp \sqrt{\omega^2 - 4}/(2j)$  when  $\omega > 2$  ( $\omega < -2$ ), corresponding to evanescent wave inputs (outputs) decaying toward (away from) the scatterer.

From Eq. (1), we find equal transmission amplitudes  $t_{LR} = t_{RL} = t_S$  between left and right CROWs for both propagating and evanescent waves, due to reciprocity [63,64]. For propagating waves, the scattering features are determined by  $jWI_2 = (S + I_2)^{-1} - (S^{\text{PT}} + I_2)^{-1}$  with

$W \equiv [\omega(1 - \frac{1}{2}c^2) - \Delta_0]/(c^2 \sin k)$  and  $S^{\text{PT}} \equiv PTSPT$ , which follows directly from Eq. (1) and the anti-PT symmetry of the scatterer, implying that, independent from the specific properties captured by  $W$ , there is a relation between the transmission coefficient  $t_S$  and the left and right reflection coefficients  $r_L$  and  $r_R$ :  $(r_R^* - r_L^*)/t_S^* = (r_L - r_R)/t_S$ . In the special scenario when  $\gamma = 0$  and thus the anti-PT-symmetric Hamiltonian  $H^{(\text{APT})}$  also satisfies the commutator relationship  $[H^{(\text{APT})}, \sigma_z T] = 0$  with  $\sigma_z = \begin{pmatrix} 1 & 0 \\ 0 & -1 \end{pmatrix}$ , we find  $|r_L|^2 - |t_S|^2 = 1$  and  $t_S r_R^* = r_L t_S^*$  [65].

Quite interestingly, for evanescent waves the scattering response can become PT symmetric, despite the absence of gain in the system. To show this feature, we set  $\omega = \Delta_0/(1 - \frac{1}{2}c^2) > 2$ , operating the CROWs at cutoff, and consequently the  $S$  matrix in Eq. (1) becomes

$$S = -I_2 - 2jc_r [-\gamma I_2 - H^{(\text{PT})} - jc_r I_2]^{-1}, \quad (2)$$

where  $c_r \equiv c^2 \sqrt{\omega^2 - 4}/2$ , and the effective Hamiltonian  $H^{(\text{PT})} \equiv \begin{pmatrix} -j\Delta & -\kappa \\ -\kappa & j\Delta \end{pmatrix}$  is PT symmetric, obeying the commutator relationship  $[H^{(\text{PT})}, \text{PT}] = 0$ . The  $S$  matrix in Eq. (2) satisfies the fundamental relation  $S^{\text{PT}} = S^{-1}$ , interestingly supporting PT-symmetric scattering at the (angular) frequency  $-\gamma \in \mathcal{R}$ , with emerging non-Hermiticity parameters (effective gain and loss) determined by the frequency detuning  $\Delta$ . Yet, the physical structure is fully passive for  $\gamma \geq |\kappa|$  [55]. The fact that evanescent waves may enable tailored PT-symmetric phenomena without requiring gain can be heuristically explained considering that reflection and transmission coefficients for evanescent waves are not bound by power conservation, since unidirectional evanescent waves do not transport energy. Reflection and transmission coefficients larger than unity in complementary bilayers, as in Fig. 1(b), have been shown to enable subdiffractive focusing and anomalous transparency phenomena [66,67], and we connect our findings to the unusual physics of these systems below.

In the CROW setup of Fig. 1(a), the PT-symmetric Hamiltonian for evanescent waves implies features commonly found for propagating waves in systems with balanced gain and loss [4]. For instance, despite the fact that our system is fully passive, in the following we show that it can enable ATRs and PT-symmetric phase transitions, which cannot be achieved in passive systems excited by propagating signals because of power conservation [25–27]. ATR implies unimodular transmission in both directions, and at the same time zero reflection only from one side, a response that is forbidden in passive systems. Since evanescent waves do not carry energy on their own, and energy flow only arises in the presence of two evanescent waves decaying in opposite directions [55],

the ATR phenomenon not only is allowed in our scenario, but it also exhibits intriguing new features in terms of energy transfer compared to ordinary PT-symmetric systems. While for excitation from one side, ATR for evanescent waves completely suppresses reflection and thus energy flow, from the opposite port the ATR induces a strong reflection and thus opens a channel for unidirectional energy flow, offering unique opportunities for robust near-field energy transfer and sensors that are bound to extract energy only from the side of the object to be sensed.

In our structure excited with evanescent inputs, the condition  $r_R = 0$  combined with passivity and Eq. (2) requires the matching conditions  $\gamma = \kappa$  and  $\Delta = c_r$ . In this scenario, indeed we find an ATR, with transmission  $t_S = 1$  and left reflection  $r_L = 2jc_r/\kappa$ . Note that the  $S$  matrix in Eq. (2), and thus the scattering parameters, univocally depend on three ratios:  $\hat{\Delta} \equiv \Delta/\kappa$ ,  $\gamma/\kappa$ , and  $c_r/\kappa$ . In Fig. 2(a), we fix  $\gamma/\kappa = c_r/\kappa = 1$ , and show the evolution of  $r_L$ ,  $r_R$ , and  $t_S$  in the complex plane as a function of  $\hat{\Delta} \in (0, 6)$  (see color bar). When  $\hat{\Delta} = 0$  (symmetric scatterer), the left and right reflections are equal, as expected,  $r_L = r_R = (1 + 2j)/5$ , which is crossed by the trajectory of  $t_S$  at  $\hat{\Delta} = \sqrt{5}$ . The ATR ( $t_S = 1$ ,  $r_R = 0$ , and  $r_L = 2j$ ) occurs for  $\hat{\Delta} = 1$  (red arrows), for which the magnitude of  $r_L$  is larger than unity.

As we vary the frequency detuning  $\Delta$  from  $\Delta^2 < \kappa^2$  to  $\Delta^2 > \kappa^2$ , the scatterer in Fig. 1(a) transitions from its PT-symmetric phase to the PT-symmetry-broken phase, depending on whether the eigenstates of  $H_{\text{eff}}$  (or equivalently  $H^{(\text{APT})}$ ) are individually eigenstates of the PT operator [18]. Interestingly, by exploiting evanescent wave excitations, this precise phase transition can be demonstrated in a fully passive scenario for any  $\gamma \geq |\kappa|$  [55].

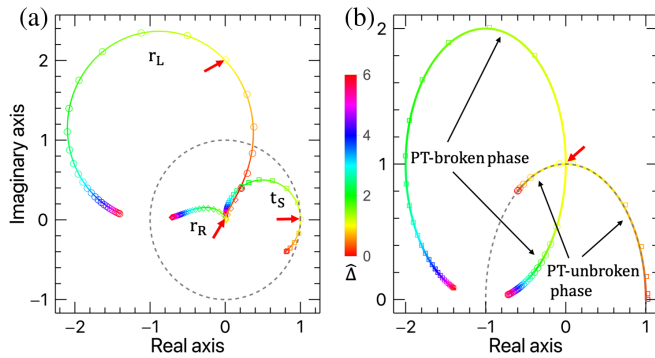


FIG. 2. Effective PT-symmetric response for evanescent waves in Fig. 1(a): variations in the complex plane of (a) scattering parameters and (b) eigenvalues, associated with the  $S$  matrix in Eq. (2), as  $\hat{\Delta}$  increases from 0 to 6, see the color bar. Red arrows indicate  $\hat{\Delta} = 1$  and the black dashed lines represent reference unit circles centered at the origin. Other parameters are  $\gamma/\kappa = c_r/\kappa = 1$ . In the same figure, the corresponding results retrieved from ADS simulation of a fully passive circuit corresponding to Fig. 1(a)[55], are indicated by various symbols.

Correspondingly, in this evanescent wave regime our system supports the typical scattering phase transition of PT-symmetric systems, arising when the eigenvalues of  $S$  in Eq. (2) go through an EP, going from being an individually unimodular (PT-unbroken phase) to an inverse-conjugate pair (PT-broken phase) [7,68]. The evolution of the eigenvalues of  $S$  with  $\hat{\Delta} \in (0, 6)$  is shown in Fig. 2(b), highlighting the emergence of an EP and a phase transition, occurring at  $\hat{\Delta} = \pm 1$  independent of the specific values of  $\gamma/\kappa$  and  $c_r/\kappa$ .

In order to verify these predictions in a realistic system, we performed full-wave simulations of a *fully passive* electronic circuit implementing the response of Fig. 1(a) using Advanced Design System (ADS), as detailed in [55]. The retrieved scattering coefficients and eigenvalues are shown in Fig. 2 with symbols, in clear agreement with the theoretical predictions based on our Hamiltonian model. The simulation details together with the steady-state time dependent signals and field profiles at the ATR point are given in [55]. At the phase transition, a sublinear variation of the eigenvalue dispersion with  $\hat{\Delta}$  indicates interesting opportunities for sensing, as achieved in several PT-symmetric scenarios in recent years [69–71]. Yet, here the considered geometry with  $\gamma = \kappa > 0$  is fully passive, and PT symmetry is enabled by its excitation with evanescent waves. This opens unique opportunities for noninvasive near-field sensing with superior performance.

*Scattering of evanescent waves in anti-PT symmetric photonic heterostructures.*—Having determined how evanescent waves can enable PT-symmetric features when exciting suitably tailored passive systems, we turn our attention to photonic heterostructures that may enable this functionality in free space (with permittivity  $\epsilon_0$  and permeability  $\mu_0$ ), in connection with the geometry in Fig. 1(b) and with a broad range of near-field imaging setups. We assume a pair of conjugate slabs [66], for instance a double-positive slab with a balanced double-negative slab of equal thickness  $h$ , with relative permittivity and permeability  $\epsilon_1 = \epsilon' - j\epsilon''$ ,  $\mu_1 = \mu' - j\mu''$  and  $\epsilon_2 = -\epsilon' - j\epsilon''$ ,  $\mu_2 = -\mu' - j\mu''$ , where both  $\epsilon'$  and  $\mu''$  are positive. This structure generalizes the scenario considered in Pendry's superlens by incorporating an equal level of material loss [ $\epsilon'', \mu'' > 0$ ] or gain [67], corresponding to the first proposal of an anti-PT symmetric structure [15].

Without loss of generality, consider now the excitation of this system by transverse-electric waves incident in the  $xz$  plane [55]. The total transfer matrix  $M_{\text{tot}}$  can be written as [55]

$$M_{\text{tot}} = L^{-1}P^{(2)}P^{(1)}L, \quad (3)$$

obtained from the continuity of the tangential electric and magnetic fields, and it involves the multiplication of

the transmission matrices  $P^{(n)}$  of each slab  $n = 1, 2$  with the resolving matrix  $L$  (and its inverse  $L^{-1}$ ) for the tangential fields. For evanescent wave excitation, the background axial wave number  $k_z^{(0)} = -j\omega\hat{\beta}/c_0$  with  $\hat{\beta} \equiv \sqrt{(k_x c_0/\omega)^2 - 1} > 0$ ,  $c_0 = 1/\sqrt{\mu_0\epsilon_0}$  and  $k_x \in \mathcal{R}$  being the transverse wave number. In this case,  $M_{\text{tot}}$  in Eq. (3) can be written as

$$M_{\text{tot}} = \begin{pmatrix} a^* & -jb \\ jp & a \end{pmatrix}, \quad (4)$$

where the elements  $b, p \in \mathcal{R}$ ,  $a \in \mathcal{C}$ , related by  $|a|^2 - bp = 1$ , i.e.,  $\det M_{\text{tot}} = 1$ , stemming from reciprocity. Like in the previous example, the system supports a PT-symmetric scattering response for evanescent

waves, with the corresponding scattering matrix  $S = \begin{pmatrix} -jp/a & 1/a \\ 1/a & -jb/a \end{pmatrix}$  obeying  $S^{\text{PT}} = S^{-1}$ . Surprisingly, for the photonic heterostructure in Fig. 1(b), this result is valid irrespective of any specific value of  $\{\hat{\beta}, \epsilon', \mu', \epsilon'', \mu''\}$  [72], including the scenario with  $\epsilon' < 0$  and  $\mu' > 0$  corresponding to paired epsilon-negative and mu-negative layers [66], and holding also for transverse-magnetic evanescent waves.

We proceed to explore the ATR phenomenon for evanescent waves in this setup. To this end, we notice that  $r_L \equiv -jp/a = 0$  requires that the transmission amplitude  $|t_S| \equiv |1/a| = 1$ . Correspondingly, the reflection asymmetry  $\Delta r \equiv |r_R - r_L|$  with right reflection  $r_R \equiv -jb/a$  is found to be

$$\Delta r = \left| \frac{2(k'\mu'' - k''\mu')(k'\mu' + k''\mu'')[\cos(2k'\hat{h}) - \cosh(2k''\hat{h})]}{(k'^2 + k''^2)(\mu'^2 + \mu''^2)} \right|, \quad (5)$$

where  $k'$  and  $k''$  are the real and imaginary parts of the (normalized) axial wave numbers  $\hat{k}_z^{(1,2)} \equiv k_z^{(1,2)} c_0/\omega = k' \mp jk''$  [with  $k_z^{(n)} = \sqrt{\epsilon_n \mu_n \omega^2/c_0^2 - k_x^2}$ ] in the  $n = 1, 2$  slab of normalized thickness  $\hat{h} \equiv h\omega/c_0$ . In the special scenario corresponding to Pendry's superlens, when the material loss or gain is zero, i.e.,  $\epsilon'' = \mu'' = 0$ , the reflection asymmetry  $\Delta r = 0$ , since in this case  $\hat{k}_z^{(1)} = \sqrt{\epsilon'\mu' - 1 - \hat{\beta}^2}$  and thus either  $k'$  or  $k''$  is also zero. Indeed, for Pendry's superlens, both left and right reflection  $r_{L,R} = 0$  and the transmission amplitude  $t_S = 1$  with zero phase delay, as confirmed by Eq. (3) after realizing that  $P^{(2)}P^{(1)} = I_2$  when  $\epsilon'' = \mu'' = 0$ . More generally, this result shows that the unusual response of conjugate materials when excited with evanescent waves, including the evanescent growth responsible for subdiffraction

imaging [73], can be directly connected with the effective PT-symmetric features of these systems and their ATR features supported by evanescent wave excitation of anti-PT-symmetric structures [74]. Conversely, we envision that the connection highlighted here can extend the functionality of metamaterial superlenses to non-Hermitian scenarios with loss (or gain), and provide new strategies for near-field imaging in diverse platforms based on PT-symmetry for evanescent waves.

To gain further insights into the ATR phenomenon in this structure, we study the case  $\mu' = \epsilon' \geq 1$  and  $\hat{\beta} = \hat{\beta}_{\text{ATR}} = \sqrt{\epsilon'^2 - \epsilon''\mu'' - 1} > 0$ , which results in  $k'' = k' = \sqrt{\epsilon'(\epsilon'' + \mu'')}/\sqrt{2}$ . As before, we set the left reflection  $r_L = 0$ . For weak loss or gain, i.e.,  $|\epsilon''/\epsilon'| \ll 1$  and  $|\mu''/\mu'| \ll 1$ , we obtain the ATR for  $\mu'' = \mu''_{\text{ATR}}$

$$\mu''_{\text{ATR}} \approx \epsilon'' \left[ \frac{3(\epsilon'^2 - 1)}{3(1 - \sqrt{\epsilon'^2 - 1}\hat{h}\epsilon') + (\epsilon'^2 - 1)(3 + \hat{h}^2\epsilon'^2)} - 1 \right]. \quad (6)$$

In Fig. 3(a),  $\mu''_{\text{ATR}}$  is plotted for  $\hat{h} = 1$  against its numerically calculated value. As expected, near the edge where  $\epsilon''$  is comparable with  $\epsilon'$ , Eq. (6) deviates more strongly. Interestingly, we find that the required  $\mu''_{\text{ATR}}$  for ATR is negative, indicating that here the structure requires gain. In addition,  $\mu''_{\text{ATR}}$  and the corresponding reflection asymmetry  $\Delta r$  at the ATR, shown in Fig. 3(b), approach zero together with  $\epsilon''$  regardless of the specific value of  $\epsilon'$ , yielding the scenario of lossless conjugate slabs, like in Pendry's superlens.

Finally, we show PT-symmetric phase transitions in the setup of Fig. 1(b) with  $\hat{h} = 1$  by varying the (normalized) decay rate  $\hat{\beta}$  of the evanescent inputs, which can be controlled by the transverse wave number  $k_x$ . For this demonstration, we fix  $\epsilon' = 1.5$  and pick the specific value

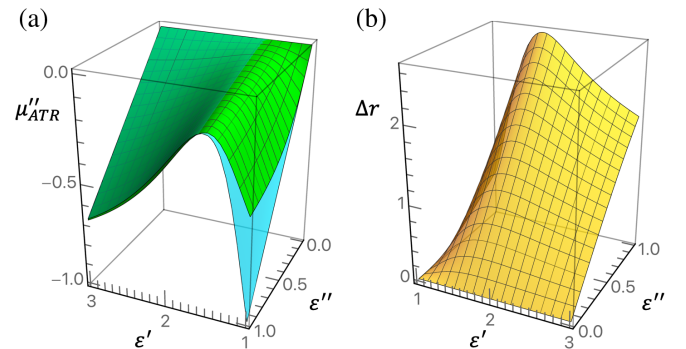


FIG. 3. 3D plots of (a) the required  $\mu''_{\text{ATR}}$  and (b) the corresponding reflection asymmetry  $\Delta r$  at ATRs versus  $\epsilon'$  and  $\epsilon''$  for evanescent waves in Fig. 1(b). In (a), the unmeshed cyan surface denotes the approximated  $\mu''_{\text{ATR}}$  using Eq. (6). Other common parameters are  $\mu' = \epsilon'$ ,  $\hat{\beta} = \hat{\beta}_{\text{ATR}} = \sqrt{\epsilon'^2 - \epsilon''\mu''_{\text{ATR}} - 1}$ , and  $\hat{h} = 1$ .

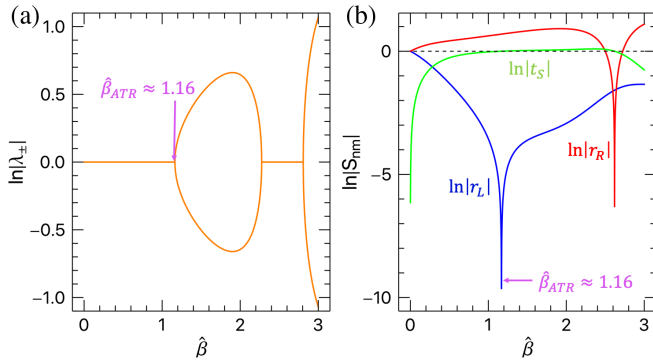


FIG. 4. Effective PT-symmetric response for evanescent waves in Fig. 1(b). Logarithm of the magnitude of (a) the eigenvalues  $\lambda_{\pm}$  and (b) the scattering parameters associated with the  $S$  matrix versus  $\hat{\beta}$ . In both (a) and (b),  $\hat{\beta}_{\text{ATR}} \approx 1.16$  for the designed ATR is indicated by the purple arrows. Other common parameters are  $\mu' = \epsilon' = 1.5$ ,  $\epsilon'' = 0.803$ ,  $\mu'' = \mu''_{\text{ATR}} \approx -0.133$ , and  $\hat{h} = 1$ .

$\epsilon'' \approx 0.803$ , such that an ATR with reflection asymmetry  $\Delta r = 2$  [see Fig. 3(b)] occurs at  $\mu'' = \mu''_{\text{ATR}} \approx -0.133$  and  $\hat{\beta} = \hat{\beta}_{\text{ATR}} \approx 1.16$ . The ATR coincides with an EP at the phase transition, as seen in Fig. 4(a), which shows the logarithm of the eigenvalue amplitude  $|\lambda_{\pm}|$  of the  $S$  matrix versus  $\hat{\beta}$ . Distinct from the previous scenarios in Fig. 2(b), the  $S$  matrix here reenters the symmetric phase, corresponding to  $\ln|\lambda_{\pm}| = 0$ , after a region of broken symmetry as we increase  $\hat{\beta}$ . In Fig. 4(b), we show the corresponding variation of the scattering parameters with respect to  $\hat{\beta}$ . Besides the designed ATR response at  $\hat{\beta} = \hat{\beta}_{\text{ATR}} \approx 1.16$ , the system experiences a second ATR at  $\hat{\beta} \approx 2.6$  with reversed response, i.e., zero reflection from the right  $r_R = 0$  and a finite left reflection  $\ln|r_L| \approx -1.6$ . Noticeably, the near-unitary transmission  $|t_S|$  and weak reflection  $|r_L|$  are robust in terms of  $\hat{\beta}$ , of great interest for near-field imaging, as it can apply to a wide range of transverse wave numbers for high-resolution images.

**Conclusions.**—We have shown how the near-field excitation of anti-PT symmetric systems can support PT-symmetric responses through the interaction with evanescent waves, overcoming the requirement of balanced loss and gain. Using two representative anti-PT symmetric structures involving coupled resonators and photonic heterostructures, we have shown that the landmarks of PT-symmetric responses can be unveiled by evanescent wave excitations, demonstrating ATRs and scattering phase transitions and verifying our predictions in a realistic fully passive circuit using full-wave simulations. We have also shown how the unusual physics of conjugate slabs, supporting negative refraction and evanescent growth, can be described in the framework of non-Hermitian physics, generalizing the response of Pendry's superlens for evanescent waves to scenarios in which loss (or gain) can enable additional interesting features typical of PT-symmetric

scenarios. These concepts open interesting possibilities for evanescent wave manipulation, extending the machinery of PT-symmetry and non-Hermitian physics to near-field optics and acoustics, for applications in sensing, imaging and communications. In addition, these findings offer a new playground to test PT-symmetry phenomena in inherently stable platforms by simply exciting them with evanescent fields.

This work was supported by the Office of Naval Research with Grant No. N00014-19-1-2011 and the Simons Foundation.

\*Corresponding author.  
aalu@gc.cuny.edu

- [1] C. M. Bender and S. Boettcher, Real Spectra in Non-Hermitian Hamiltonians Having PT Symmetry, *Phys. Rev. Lett.* **80**, 5243 (1998).
- [2] S. Assaworrorarit, X. Yu, and S. Fan, Robust wireless power transfer using a nonlinear parity-time-symmetric circuit, *Nature (London)* **546**, 387 (2017).
- [3] Z. Lin, H. Ramezani, T. Eichelkraut, T. Kottos, H. Cao, and D. N. Christodoulides, Unidirectional Invisibility Induced by PT-Symmetric Periodic Structures, *Phys. Rev. Lett.* **106**, 213901 (2011).
- [4] L. Ge, Y. D. Chong, and A. D. Stone, Conservation relations and anisotropic transmission resonances in one-dimensional PT-symmetric photonic heterostructures, *Phys. Rev. A* **85**, 023802 (2012).
- [5] L. Feng, Y.-L. Xu, W. S. Fegadolli, M.-H. Lu, J. E. B. Oliveira, V. R. Almeida, Y.-F. Chen, and A. Scherer, Experimental demonstration of a unidirectional reflectionless parity-time metamaterial at optical frequencies, *Nat. Mater.* **12**, 108 (2013).
- [6] S. Longhi, PT-symmetric laser absorber, *Phys. Rev. A* **82**, 031801(R) (2010).
- [7] Y. D. Chong, L. Ge, and A. D. Stone, PT-Symmetry Breaking and Laser-Absorber Modes in Optical Scattering Systems, *Phys. Rev. Lett.* **106**, 093902 (2011).
- [8] A. Regensburger, C. Bersch, M. A. Miri, G. Onishchukov, D. N. Christodoulides, and U. Peschel, Parity-time synthetic photonic lattices, *Nature (London)* **488**, 167 (2012).
- [9] H. Benisty *et al.*, Implementation of PT symmetric devices using plasmonics: Principle and applications, *Opt. Express* **19**, 18004 (2011).
- [10] H. Alaeian and J. A. Dionne, Parity-time-symmetric plasmonic metamaterials, *Phys. Rev. A* **89**, 033829 (2014).
- [11] M. Kang, F. Liu, and J. Li, Effective spontaneous PT-symmetry breaking in hybridized metamaterials, *Phys. Rev. A* **87**, 053824 (2013).
- [12] R. Fleury, D. L. Sounas, and A. Alù, Negative Refraction and Planar Focusing Based on Parity-Time Symmetric Metasurfaces, *Phys. Rev. Lett.* **113**, 023903 (2014).
- [13] M. Lawrence, N. Xu, X. Zhang, L. Cong, J. Han, W. Zhang, and S. Zhang, Manifestation of PT Symmetry Breaking in Polarization Space with Terahertz Metasurfaces, *Phys. Rev. Lett.* **113**, 093901 (2014).

- [14] D. Christodoulides and J. Yang, *Parity-Time Symmetry and Its Applications* (Springer, Berlin, 2018).
- [15] L. Ge and H. E. Türeci, Antisymmetric PT-phonic structures with balanced positive- and negative-index materials, *Phys. Rev. A* **88**, 053810 (2013).
- [16] J.-H. Wu, M. Artoni, and G. C. La Rocca, Non-Hermitian Degeneracies, and Unidirectional Reflectionless Atomic Lattices, *Phys. Rev. Lett.* **113**, 123004 (2014).
- [17] D. A. Antonosyan, A. S. Solntsev, and A. A. Sukhorukov, Parity-time anti-symmetric parametric amplifier, *Opt. Lett.* **40**, 4575 (2015).
- [18] F. Yang, Y.-C. Liu, and L. You, Anti-PT symmetry in dissipatively coupled optical systems, *Phys. Rev. A* **96**, 053845 (2017).
- [19] Y. Choi, C. Hahn, J. W. Yoon, and S. H. Song, Observation of an anti-PT-symmetric exceptional point and energy-difference conserving dynamics in electrical circuit resonators, *Nat. Commun.* **9**, 2182 (2018).
- [20] X.-L. Zhang, T. Jiang, and C. T. Chan, Dynamically encircling an exceptional point in anti-parity-time symmetric systems: Asymmetric mode switching for symmetry-broken modes, *Light Sci. Appl.* **8**, 1 (2019).
- [21] P. Peng, W. Cao, C. Shen, W. Qu, J. Wen, L. Jiang, and Y. Xiao, Anti-parity-time symmetry with flying atoms, *Nat. Phys.* **12**, 1139 (2016).
- [22] Y. Li, Y.-G. Peng, L. Han, M.-A. Miri, W. Li, M. Xiao, X.-F. Zhu, J. Zhao, A. Alù, S. Fan, and C.-W. Qiu, Anti-parity-time symmetry in diffusive systems, *Science* **364**, 170 (2019).
- [23] F. X. Zhang, Y. M. Feng, X. F. Chen, L. Ge, and W. J. Wan, Synthetic Anti-PT Symmetry in a Single Microcavity, *Phys. Rev. Lett.* **124**, 053901 (2020).
- [24] A. Bergman, R. Duggan, K. Sharma, M. Tur, A. Zadok, and A. Alù, Observation of anti-parity-time-symmetry, phase transitions and exceptional points in an optical fibre, *Nat. Commun.* **12**, 486 (2021).
- [25] M. Ornigotti and A. Szameit, Quasi PT-symmetry in passive photonic lattices, *J. Opt.* **16**, 065501 (2014).
- [26] A. Guo, G. J. Salamo, D. Duchesne, R. Morandotti, M. Volatier-Ravat, V. Aimez, G. A. Siviloglou, and D. N. Christodoulides, Observation of PT-Symmetry Breaking in Complex Optical Potentials, *Phys. Rev. Lett.* **103**, 093902 (2009).
- [27] Y. N. Joglekar and A. K. Harter, Passive parity-time-symmetry-breaking transitions without exceptional points in dissipative photonic systems, *Photonics Res.* **6**, A51 (2018).
- [28] C. Girard, C. Joachim, and S. Gauthier, The physics of the near-field, *Rep. Prog. Phys.* **63**, 893 (2000).
- [29] E. Betzig and J. K. Trautman, Near-field optics: Microscopy, spectroscopy, and surface modification beyond the diffraction limit, *Science* **257**, 189 (1992).
- [30] D. Polder and M. Van Hove, Theory of radiative heat transfer between closely spaced bodies, *Phys. Rev. B* **4**, 3303 (1971).
- [31] J. B. Pendry, Radiative exchange of heat between nanostructures, *J. Phys. Condens. Matter* **11**, 6621 (1999).
- [32] A. I. Volokitin and B. N. J. Persson, Near-field radiative heat transfer and noncontact friction, *Rev. Mod. Phys.* **79**, 1291 (2007).
- [33] L. Hu, A. Narayanaswamy, X. Chen, and G. Chen, Near-field thermal radiation between two closely spaced glass plates exceeding Planck's blackbody radiation law, *Appl. Phys. Lett.* **92**, 133106 (2008).
- [34] P. Ben-Abdallah and K. Joulain, Fundamental limits for noncontact transfers between two bodies, *Phys. Rev. B* **82**, 121419(R) (2010).
- [35] S.-A. Biehs, M. Tschikin, and P. Ben-Abdallah, Hyperbolic Metamaterials as an Analog of a Blackbody in the Near Field, *Phys. Rev. Lett.* **109**, 104301 (2012).
- [36] O. D. Miller, S. G. Johnson, and A. W. Rodriguez, Shape-Independent Limits to Near-Field Radiative Heat Transfer, *Phys. Rev. Lett.* **115**, 204302 (2015).
- [37] K. Kim, B. Song, V. Fernández-Hurtado, W. Lee, W. Jeong, L. Cui, D. Thompson, J. Feist, M. T. H. Reid, F. J. García-Vidal, J. C. Cuevas, E. Meyhofer, and P. Reddy, Radiative heat transfer in the extreme near field, *Nature (London)* **528**, 387 (2015).
- [38] S. Basu, Z. M. Zhang, and C. J. Fu, Review of near-field thermal radiation and its application to energy conversion, *Int. J. Energy Res.* **33**, 1203 (2009).
- [39] B. Zhao, K. Chen, S. Buddhiraju, G. Bhatt, M. Lipson, and S. Fan, High-performance near-field thermophotovoltaics for waste heat recovery, *Nano Energy* **41**, 344 (2017).
- [40] R. St-Gelais, G. R. Bhatt, L. Zhu, S. Fan, and M. Lipson, Hot carrier-based near-field thermophotovoltaic energy conversion, *ACS Nano* **11**, 3001 (2017).
- [41] A. Fiorino, L. Zhu, D. Thompson, R. Mittapally, P. Reddy, and E. Meyhofer, Nanogap near-field thermophotovoltaics, *Nat. Nanotechnol.* **13**, 806 (2018).
- [42] C. R. Otey, W. T. Lau, and S. Fan, Thermal Rectification Through Vacuum, *Phys. Rev. Lett.* **104**, 154301 (2010).
- [43] P. Ben-Abdallah and S.-A. Biehs, Near-Field Thermal Transistor, *Phys. Rev. Lett.* **112**, 044301 (2014).
- [44] A. Fiorino, D. Thompson, L. Zhu, R. Mittapally, S.-A. Biehs, O. Bezencenet, N. El-Bondry, S. Bansropun, P. Ben-Abdallah, E. Meyhofer, and P. Reddy, A thermal diode based on nanoscale thermal radiation, *ACS Nano* **12**, 5774 (2018).
- [45] Y. Long, J. Ren, and H. Chen, Intrinsic spin of elastic waves, *Proc. Natl. Acad. Sci. U.S.A.* **115**, 9951 (2018).
- [46] I. D. Toftul, K. Y. Bliokh, M. I. Petrov, and F. Nori, Acoustic Radiation Force and Torque on Small Particles as Measures of the Canonical Momentum and Spin Densities, *Phys. Rev. Lett.* **123**, 183901 (2019).
- [47] C. Shi, R. Zhao, Y. Long, S. Yang, Y. Wang, H. Chen, J. Ren, and X. Zhang, Observation of acoustic spin, *Natl. Sci. Rev.* **6**, 707 (2019).
- [48] K. Y. Bliokh and F. Nori, Transverse spin and surface waves in acoustic metamaterials, *Phys. Rev. B* **99**, 020301(R) (2019).
- [49] Y. Long, H. Ge, D. Zhang, X. Xu, J. Ren, M.-H. Lu, M. Bao, H. Chen, and Y.-F. Chen, Symmetry selective directionality in near-field acoustics, *Natl. Sci. Rev.* **7**, 1024 (2020).
- [50] L. Wei and F. J. Rodríguez-Fortuño, Far-field and near-field directionality in acoustic scattering, *New J. Phys.* **22**, 083016 (2020).
- [51] H. Li, A. Mekawy, A. Krasnok, and A. Alù, Virtual Parity-Time Symmetry, *Phys. Rev. Lett.* **124**, 193901 (2020).

- [52] H. Li, H. Moussa, D. Sounas, and A. Alù, Parity-Time Symmetry Based on Time Modulation, *Phys. Rev. Applied* **14**, 031002(R) (2020).
- [53] A. Yariv, Y. Xu, R. K. Lee, and A. Scherer, Coupled-resonator optical waveguide: A proposal and analysis, *Opt. Lett.* **24**, 711 (1999).
- [54] J. K. S. Poon and A. Yariv, Active coupled-resonator optical waveguides. I. Gain enhancement and noise, *J. Opt. Soc. Am. B* **24**, 2378 (2007).
- [55] See Supplemental Material at <http://link.aps.org/supplemental/10.1103/PhysRevLett.127.014301> for details on the implementation of non-Hermitian imaginary coupling in electrical circuits, the circuit simulation implementing anti-PT-symmetric coupled resonators, and the derivation of the total transfer matrix  $M_{\text{tot}}$  in photonic heterostructures, which includes Refs. [51,56–58].
- [56] J. Schindler, A. Li, M. C. Zheng, F. M. Ellis, and T. Kottos, Experimental study of active LRC circuits with PT symmetries, *Phys. Rev. A* **84**, 040101(R) (2011).
- [57] M. Chitsazi, H. Li, F. M. Ellis, and T. Kottos, Experimental Realization of Floquet PT-Symmetric Systems, *Phys. Rev. Lett.* **119**, 093901 (2017).
- [58] D. W. Berreman, Optics in stratified and anisotropic media:  $4 \times 4$ -matrix formulation, *J. Opt. Soc. Am.* **62**, 502 (1972).
- [59] S. Longhi, Non-Hermitian tight-binding network engineering, *Phys. Rev. A* **93**, 022102 (2016).
- [60] R. Carminati, J. J. Sáenz, J.-J. Greffet, and M. Nieto-Vesperinas, Reciprocity, unitarity, and time-reversal symmetry of the  $S$  matrix of fields containing evanescent components, *Phys. Rev. A* **62**, 012712 (2000).
- [61] A. Krasnok, D. Baranov, H. Li, M.-A. Miri, F. Monticone, and A. Alù, Anomalies in light scattering, *Adv. Opt. Photonics* **11**, 892 (2019).
- [62] Note that, like the incident frequency  $\omega$ , both the scatterer-lead coupling  $c$  and the effective Hamiltonian  $H_{\text{eff}}$  are given in units of interresonator coupling coefficient in CROWs.
- [63] R. Carminati, M. Nieto-Vesperinas, and J.-J. Greffet, Reciprocity of evanescent electromagnetic wave, *J. Opt. Soc. Am. A* **15**, 706 (1998).
- [64] G. K. Svendsen, M. W. Haakestad, and J. Skaar, Reciprocity and the scattering matrix of waveguide modes, *Phys. Rev. A* **87**, 013838 (2013).
- [65] L. Jin, Scattering properties of a parity-time-antisymmetric non-Hermitian system, *Phys. Rev. A* **98**, 022117 (2018).
- [66] A. Alù and N. Engheta, Pairing an epsilon-negative slab with a mu-negative slab: Resonance, tunneling and transparency, *IEEE Trans. Antennas Propag.* **51**, 2558 (2003).
- [67] J. B. Pendry, Negative Refraction Makes a Perfect Lens, *Phys. Rev. Lett.* **85**, 3966 (2000).
- [68] P. Ambichl, K. G. Makris, L. Ge, Y. D. Chong, A. D. Stone, and S. Rotter, Breaking of PT Symmetry in Bounded and Unbounded Scattering Systems, *Phys. Rev. X* **3**, 041030 (2013).
- [69] Z.-P. Liu, J. Zhang, Ş. K. Özdemir, B. Peng, H. Jing, X.-Y. Lü, C.-W. Li, L. Yang, F. Nori, and Y.-x. Liu, Metrology with PT-Symmetric Cavities: Enhanced Sensitivity near the PT-Phase Transition, *Phys. Rev. Lett.* **117**, 110802 (2016).
- [70] P.-Y. Chen, M. Sakhdari, M. Hajizadegan, Q. Cui, M. M.-C. Cheng, R. El-Ganainy, and A. Alù, Generalized parity-time symmetry condition for enhanced sensor telemetry, *National electronics review* **1**, 297 (2018).
- [71] Z. Xiao, H. Li, T. Kottos, and A. Alù, Enhanced Sensing and Nondegraded Thermal Noise Performance Based on PT-Symmetric Electronic Circuits with a Sixth-Order Exceptional Point, *Phys. Rev. Lett.* **123**, 213901 (2019).
- [72] We also point out that for the scattering of evanescent waves in reciprocal PT-symmetric systems, the special relationships  $r_L = r_R^*$  and  $\text{Im}(t_S) = 0$  among scattering parameters exist, which is identical to the scattering properties for propagating waves in the anti-PT heterostructures given in Ref. [15].
- [73] A. Alù and N. Engheta, Physical Insight into the “Growing” Evanescent Fields of Double-Negative Metamaterial Lenses Using their Circuit Equivalence, *IEEE Trans. Antennas Propag.* **54**, 268 (2006).
- [74] Interestingly, negative refraction and planar focusing exhibited in Pendry’s superlens were shown based on PT-symmetric metasurfaces before, see Ref. [12].